文章编号：1001-9014(XXXX)XX-0001-06

DOI:10.11972/j.issn.1001-9014.XXXX.XX.001

Characteristic analysis of 1.06 μm long-cavity diode lasers based on asymmetric waveguide structures

ZHAO Ren-Ze, GAO Xin, FU Ding-Yang, ZHANG Yue, SU Peng, BO Bao-Xue*

(National Key Lab of High Power Semiconductor Lasers, Changchun University of Science and Technology, Changchun 130022, China)

Abstract: In long-cavity edge-emitting diode lasers, longitudinal spatial hole burning (LSHB), two-photon absorption (TPA) and free carrier absorption (FCA) are among the key factors that affect the linear increase in output power at high injection currents. In this paper, a simplified numerical analysis model is proposed for 1.06 μm long-cavity diode lasers by combining TPA and FCA losses with one-dimensional (1D) rate equations. The effects of LSHB, TPA and FCA on the output characteristics are systematically analyzed, and it is proposed that adjusting the front facet reflectivity and the position of the quantum well (QW) in the waveguide layer can improve the front facet output power.

Key words: diode lasers, longitudinal spatial hole burning, free carrier absorption, two-photon absorption

基于非对称波导结构的1.06 μm长腔半导体激光器特性分析

赵仁泽, 高 欣, 伏丁阳, 张 悦, 苏 鹏, 薄报学*

(长春理工大学 高功率半导体激光国家重点实验室,吉林 长春 130022)

摘要:在长腔边发射二极管激光器中,纵向空间烧孔(LSHB)、双光子吸收(TPA)和自由载流子吸收(FCA)是影响高注入电流下输出功率线性增长的关键因素。针对1.06 μm长腔半导体激光器,通过将TPA和FCA损耗与一维速率方程相结合,提出一种简化数值分析模型。系统分析了LSHB、TPA和FCA对输出特性的影响,并提出可以通过调整前腔面反射率和量子阱(QW)在波导层中的位置来提高前腔面输出功率。

关 键 词:半导体激光器;纵向空间烧孔;自由载流子吸收;双光子吸收

中图分类号:TN248.4　　**文献标识码**:A

Introduction

1.06 μm diode lasers are widely used in laser fuzing, laser ranging, laser blinding and target identification. Usually, high power edge-emitting diode lasers are coated with high and low reflectivity films on both cavity facets to enhance slope efficiency. On the other hand, to reduce thermal resistance, a long cavity is adopted for high power diode lasers, which mitigates temperature rise in the active region[1]. However, the above design in practical devices can exacerbate the non-uniform distribution of carrier density along the cavity length, a phenomenon known as longitudinal spatial hole burning (LSHB)[2-3]. The LSHB can lead to an increase in threshold current and a decrease in slope efficiency[4].

Two-photon absorption (TPA) and free carrier absorption (FCA) are considered the main mechanisms limiting the output power[5, 6]. High power diode lasers tend to have a large waveguide layer[7], which is typically a few microns thick. They contain a thin active region consisting of one or more quantum well (QW) layers. The n-side waveguide is thicker than the p-side waveguide (the difusion coefficient of holes is significantly smaller than that of electrons, so the waveguide loss on the p-side tends to be more severe. A low waveguide loss caused by FCA can be achieved by reducing the p-side waveguide thickness.)

Usually, there are two types of TPA loss: (i) the di-

Received date: 2023-08-07, **revised date**: 2023-11-26　　**收稿日期**:2023-08-07,**修回日期**:2023-11-26

Foundation items: Supported by National Key R&D Project (2017YFB0405100); National Natural Science Foundation of China (61774024/61964007); Jilin province science and technology development plan (20190302007GX)

Biography: Zhao Renze(1999-), male, Nanyang, postgraduate. Research area involves high power semiconductor laser. E-mail: 1310495184@qq.com

* **Corresponding author**: E-mail: bbx@cust.edu.cn

rect light absorption loss, namely direct TPA loss; (ii) TPA will generate free carriers, which can further attenuate the light field through free carrier absorption, namely indirect TPA loss[8]. TPA loss with a symmetric waveguide has been studied using experimentally measured parameters[5, 9]. In this paper, waveguide losses including TPA loss in asymmetric waveguide structures are analyzed to optimize the output characteristics of long-cavity diode lasers, while FCA loss due to current injection is also considered.

1 Waveguide structures of lasers

The vertical waveguide structure of a typical high power diode laser is shown in Fig. 1. h is the thickness of the waveguide layer, the position of the QW in the waveguide layer is denoted as p_x and $\Psi^2(x)$ is the normalized mode field intensity distribution, $\int_{-\infty}^{+\infty}\Psi^2(x)dx = 1$. Since the QW thickness (10 nm) is much smaller than the waveguide layer in Fig. 1, the optical mode field of the device is mainly determined by the waveguide and confinement layers, which can be expressed approximately by the mode field distribution in a three-layer slab waveguide[10]:

$$\Psi(x) = \begin{cases} \frac{1}{C_0}\cos(kx - \varphi), & 0 < x < h \\ \frac{1}{C_0}cos\varphi\exp(\gamma_n x), & x < 0 \\ \frac{1}{C_0}\cos(kh - \varphi)\exp(-\gamma_p(x - h)), & x > h \end{cases} \quad (1)$$

where $k = \frac{2\pi}{\lambda}\sqrt{n_{wg}^2 - n_o^2}$ is the transverse wave vector, $\gamma_n = \frac{2\pi}{\lambda}\sqrt{n_o^2 - n_n^2}$ and $\gamma_p = \frac{2\pi}{\lambda}\sqrt{n_o^2 - n_p^2}$ are the field decrements in the n and p confinement layers, respectively. $\varphi = \arctan(\frac{\gamma_n}{k})$, and $C_0 = \sqrt{(h + \frac{1}{\gamma_n} + \frac{1}{\gamma_p})/2}$. The n_n, n_p and n_{wg} are the refractive indices of the n and p confinement layers and the waveguide layer, respectively. The effective refractive index n_o of the fundamental mode can be obtained from the transcendental equation $kh = \arctan\left(\frac{\gamma_n}{k}\right) + \arctan(\frac{\gamma_p}{k})$.

2 Theoretical model

Direct and indirect TPA losses, FCA loss due to current injection and material loss are considered for performance simulation of long-cavity diode lasers with the effect of LSHB. The direct TPA loss can be expressed as[11]:

$$\alpha_{TPA}^{direct} = \frac{P(z)}{w}\int_{-\infty}^{\infty}\beta(x)\psi^4(x)dx \quad , \quad (2)$$

here $P(z)$ is the mode power along the cavity, w is the stripe width and $\beta(x)$ is the TPA coefficient for different materials in the waveguide structure. As shown in Fig. 1, the TPA loss in the confinement layer can be neglected due to the weak mode field in the confinement layer. Previous studies have found that the contribution of QW to TPA is negligible compared to the waveguide regions[5]. So the total TPA loss is primarily contributed by the waveguide layer (GaAs). The direct TPA loss can be further simplified as:

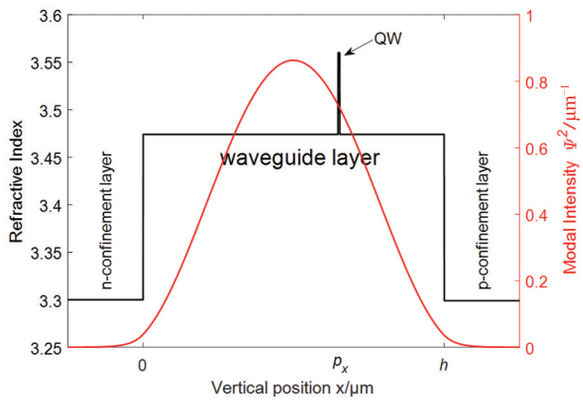

Fig. 1 Refractive index and fundamental mode intensity profiles of the vertical waveguide
图1 垂直波导的折射率和基模强度分布

$$\alpha_{TPA}^{direct} = \frac{\beta_{wg}P(z)}{w}\int_0^h\psi^4(x)dx \quad , \quad (3)$$

here β_{wg} is the TPA coefficient of the waveguide layer. In order to combine the direct TPA loss with one-dimensional (1D) rate equations, the direct TPA loss can be expressed as a function of photon density along the cavity. $P(z)$ is given as a function of photon density $N_p(z)$ by the following equation:

$$P(z) = \frac{wd}{\Gamma}v_g\frac{h_1 c}{\lambda}N_p(z) \quad , \quad (4)$$

here h_1 is Planck's constant, v_g is the group velocity of light, λ is the wavelength, c is the speed of light in vacuum and d is the QW thickness. The confinement factor Γ is expressed by the following equation:

$$\Gamma = \frac{\int_{p_x - \frac{d}{2}}^{p_x + \frac{d}{2}}\psi^2(x)dx}{\int_{-\infty}^{+\infty}\psi^2(x)dx} \quad . \quad (5)$$

Substituting Eq. (4) into Eq. (3), we obtain that:

$$\alpha_{TPA}^{direct} = \frac{\beta_{wg}dv_g h_1 c}{\Gamma\lambda}\int_0^h\psi^4(x)dxN_p(z) = \beta_{TPA}^{direct}N_p(z), \quad (6)$$

here $\beta_{TPA}^{direct} = \frac{\beta_{wg}dv_g h_1 c}{\Gamma\lambda}\int_0^h\psi^4(x)dx$, is the direct TPA coefficient. Since the waveguide layer is intentionally undoped, there is quasi-neutrality within the waveguide layer, meaning that the electron and hole have the same density, and then the carrier transport can be described by the ambipolar diffusion equation:

$$D_a \frac{\partial^2 N}{\partial^2 x} + G(x,z) - R\left(N(x,z)\right) = 0 \quad , \quad (7)$$

here $D_a = \frac{2D_e D_h}{D_e + D_h}$, D_e and D_h are the electron and hole diffusion coefficients in the waveguide layer, respectively. The indirect TPA loss is caused by the absorption of light through TPA-generated carriers. The distribution of TPA-generated carrier density can be obtained based on the TPA generation term[11]:

$$G(x,z) = \frac{\beta_{wg}\lambda}{h_1 c}\left(\frac{P(z)}{w}\right)^2 \psi^4(x) \quad . \quad (8)$$

The indirect TPA loss should be a function of photon density along the cavity length, which means $G(x,z)$ is a function of photon density. Substituting Eq. (4) into Eq. (8) gives:

$$G(x,z) = \frac{\beta_{wg} h_1 c}{\lambda}\left(\frac{dv_g}{\Gamma}\right)^2 \psi^4(x) N_p(z)^2 \quad . \quad (9)$$

Neglecting carrier recombination (R=0), the distribution of the TPA-generated carrier density in the waveguide layer is obtained by combining the boundary conditions with Eq. (7):

$$\Delta N_{TPA}(x,z) = \gamma N_p(z)^2 \quad , \quad (10)$$

here γ is a function of x and p_x for the n and p side waveguides. The indirect TPA loss is expressed as:

$$\begin{aligned} \alpha_{TPA}^{indirect} &= (\sigma_e + \sigma_h)\int_0^h \Delta N_{TPA}(x,z)\psi^2(x)dx \\ &= \int_0^h (\sigma_e + \sigma_h)\gamma\psi^2(x)dx N_p(z)^2 \\ &= \beta_{TPA}^{indirect} N_p(z)^2 \end{aligned} \quad , \quad (11)$$

here $\beta_{TPA}^{indirect} = \int_0^h (\sigma_e + \sigma_h)\gamma\psi^2(x)dx$, is the indirect TPA coefficient. σ_e and σ_h are the free-electron and free-hole absorption cross-sections, respectively. Neglecting the carrier recombination, the carrier density distribution in the waveguide layer can be obtained by Eq. (7)[6]:

$$\Delta N_j(x) = \begin{cases} \frac{j}{2eD_e}\left(p_x - \frac{d}{2} - x\right) + N_b, 0 < x < p_x - \frac{d}{2} \\ \frac{j}{2eD_h}\left(x - p_x - \frac{d}{2}\right) + N_b, p_x + \frac{d}{2} < x < h \end{cases} , \quad (12)$$

here j is the current density, e is the electron charge, $N_b \approx \frac{j}{ed}\tau$, τ is the time of carrier capture into the QW. The FCA loss in the waveguide layer can be expressed as:

$$\alpha_j^{wg} = (\sigma_e + \sigma_h)\int_0^h \Delta N_j(x)\psi^2(x)dx \quad . \quad (13)$$

The FCA loss in the QW can be expressed as:

$$\alpha_j^{QW} = \Gamma(\sigma_e + \sigma_h)N(z) = \beta_j^{QW} N(z) \quad , \quad (14)$$

here $\beta_j^{QW} = \Gamma(\sigma_e + \sigma_h)$, $N(z)$ is the carrier density in the QW. Because of LSHB, the carrier density $N(z)$ is no longer constant but decreases gradually from the rear facet to the front facet. The FCA loss in the confinement layer can be expressed as[6]:

$$\alpha_j^{cl} = \sigma_e \int_{-\infty}^{0} N_{cl}\psi^2(x)dx + \sigma_h \int_h^{+\infty} N_{cl}\psi^2(x)dx \quad , \quad (15)$$

here N_{cl} is the doping concentration of the confinement layer. The behavior of diode lasers is determined by the relationship equation between carriers and photons. In the conventional rate equations, a uniform distribution of carrier density along the cavity length is usually assumed. However, this is not the case in high power diode lasers. Considering the effect of the losses mentioned above and the inhomogeneity, the steady state 1D rate equations are modified as:

$$\frac{\eta_i j}{ed} - R_{sp}\left[N(z)\right] - v_g g\left[N(z)\right]\left[N_p^+(z) + N_p^-(z)\right] = 0 \quad , \quad (16)$$

$$\frac{dN_p^{\pm}(z)}{dz} = \pm\left\{\Gamma g\left[N(z)\right] - \alpha_i - \alpha_j^{wg} - \alpha_j^{cl} - \beta_j^{QW} N(z) - \beta_{TPA}^{direct} N_p^{\pm}(z) - \beta_{TPA}^{indirect} N_p^{\pm}(z)^2\right\} N_p^{\pm}(z) \quad . \quad (17)$$

Equation (16) describes the change in carrier density due to spontaneous and stimulated recombination under current injection. Equation (17) describes the evolution of the photon density along the laser cavity and takes into account internal losses. α_i and η_i are the material loss and internal quantum efficiency, respectively. $N_p^+(z)$ and $N_p^-(z)$ are the photon densities for forward and backward propagation, respectively. $N_p(z) = N_p^-(z) + N_p^+(z)$. $R_{sp}\left[N(z)\right] = AN(z) + BN(z)^2 + CN(z)^3$, is the spontaneous recombination rate. The gain coefficient can be expressed as $g\left[N(z)\right] = g_o \ln\left[N(z)/N_{tr}\right]$. The boundary conditions for Eqs. (16) and (17) at the rear facet ($z = 0$) and the front facet ($z = L$) are:

$$N_p^+(0) = R_{HR} N_p^-(0) \quad , \quad (18)$$

$$R_{AR} N_p^+(L) = N_p^-(L) \quad , \quad (19)$$

here L is the cavity length, R_{AR} and R_{HR} are the front and rear facet reflectivities, respectively. The photon and carrier density distribution along the laser cavity can be calculated by numerically solving Eqs. (16)-(19) by the finite difference method. The threshold lasing condition can be expressed as:

$$\frac{1}{L}\int_0^L \Gamma g\left[N(z)\right]dz = \alpha_{total} + \alpha_m \, , \quad (20)$$

here α_{total} is the total internal loss and α_m is the output loss. The threshold current can be expressed as[2]:

$$I_{th} = \frac{ewd}{\eta_i}\int_0^L R_{sp}\left[N(z)\right]dz \quad . \quad (21)$$

The front facet output power can be expressed as:

$$P_{out} = (1 - R_{AR}) v_g \frac{dw}{\Gamma}\frac{h_1 c}{\lambda} N_p^+(L) \quad . \quad (22)$$

Table 1 lists the main device parameters for the simulation calculation.

Table 1 Device parameters used
表1 所用器件参数

Symbol	Parameter	Value
λ	wavelength	1.06 μm
n_{wg}	refractive index of waveguide layer	3.474
n_n	refractive index of n-confinement layer	3.3
n_p	refractive index of p-confinement layer	3.3
β_{wg}	TPA coefficient of waveguide layer	2×10^{-8} cm/W
L	cavity length	5 mm
w	stripe width	100 μm
d	QW thickness	10 nm
R_{HR}	the rear facet reflectivity	0.99
h	waveguide layer thickness	2 μm
σ_e	free-electron absorption cross-section	3×10^{-18} cm^2
σ_h	free-hole absorption cross-section	1×10^{-17} cm^2
D_e	electron diffusion coefficient	200 cm^2 s^{-1}
D_h	hole diffusion coefficient	10 cm^2 s^{-1}
η_i	internal quantum efficiency	0.95
N_{cl}	doping concentration of confinement layer	1×10^{18} cm^{-3}
α_i	material loss	0.5 cm^{-1}
A	SRH recombination coefficient	5.88×10^8 s^{-1}
B	spontaneous emission coefficient	1×10^{-10} cm^3 s^{-1}
C	auger recombination coefficient	2×10^{-30} cm^6 s^{-1}
g_0	gain constant	2140 cm^{-1}
N_{tr}	transparency carrier density	1.77×10^{18} cm^{-3}
τ	time of carrier capture into the QW	150 fs

3 Results and analysis

Figure 2 shows β_{TPA}^{direct} and $\beta_{TPA}^{indirect}$ versus the position of QW. It can be seen that both coefficients increase gradually as p_x increases. This is because both coefficients are inversely proportional to the confinement factor, which gradually decreases as the QW shifts towards the p-side, as shown in Fig. 4.

Since the FCA and TPA losses vary with the carrier or photon density along the cavity, the average loss along the cavity is used to express the magnitude of loss. Figure 3 shows the variation of total internal loss and slope efficiency with QW positions at an injection current I = 20 A and R_{AR} = 0.01. It can be seen that the total internal loss decreases monotonically as the QW shifts towards the p-side, while the slope efficiency has an opposite trend. The FCA loss decreases as the QW shifts towards the p-side, while the TPA loss increases with the TPA coefficients $\beta_{TPA}^{indirect}$ and β_{TPA}^{direct}. However, the decrease of FCA loss is greater than the increase of TPA loss.

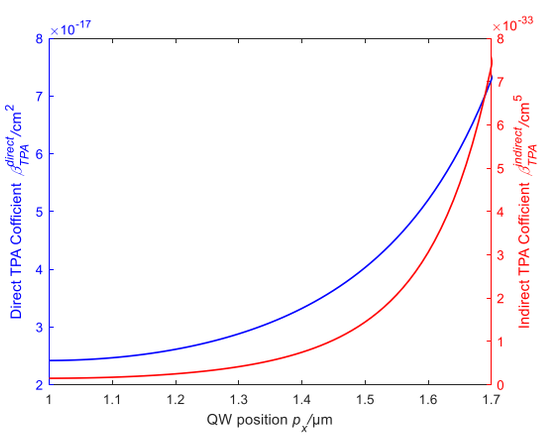

Fig. 2 The direct and indirect TPA coefficients versus QW positions
图2 直接和间接TPA系数随QW位置的变化

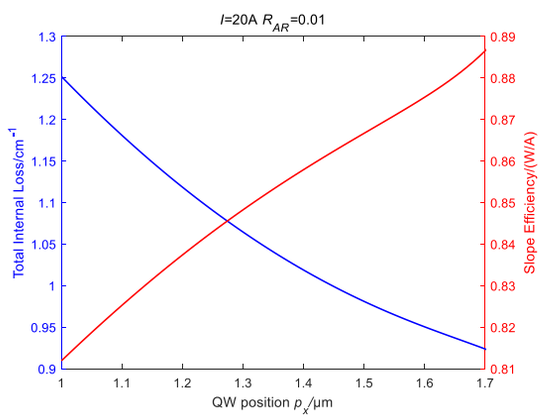

Fig. 3 Total internal loss and slope efficiency versus QW positions
图3 总内损耗和斜率效率随QW位置的变化

Figure 4 shows the variation of the confinement factor and threshold current with QW positions at I = 20 A and R_{AR} = 0.01. It can be seen that the confinement factor decreases and the threshold current increases as the QW shifts towards the p-side. From Eqs. (20) and (21), we can see that the threshold current is approximately an inverse function of the confinement factor. Though the total internal loss decreases as the QW shifts towards the p-side, the confinement factor has a greater effect on the variation trend of the threshold current.

Since the slope efficiency and threshold current exhibit the same trend when the QW shifts towards the p-

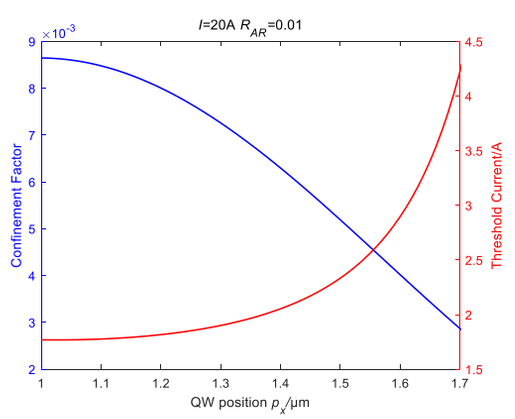

Fig. 4 Confinement factor and threshold current versus QW positions
图4 限制因子和阈值电流随QW位置的变化

side, there might be an optimal QW position that maximizes the front facet output power. Figure 5 shows the variation of the front facet output power with QW positions at I = 20 A and R_{AR} = 0.01. It can be seen that the maximum output power is achieved at p_x = 1.39 μm.

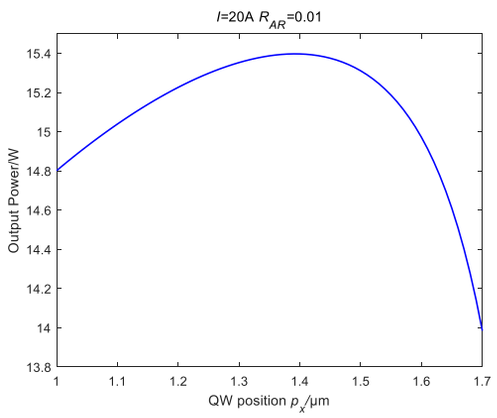

Fig. 5 Output power versus QW positions
图5 输出功率随QW位置的变化

The front facet reflectivity plays an important role in the performance of high power diode lasers. Figure 6 shows the optimized front facet output power and the corresponding QW position versus different front facet reflectivities at I = 20 A. It can be seen that the output power initially increases and then decreases, while the optimal QW position gradually shifts towards the n-side as the front facet reflectivity decreases. This is because an appropriate reduction in the front facet reflectivity can improve the slope efficiency. However, if the reflectivity is too low, it will cause severe LSHB, resulting in a reduction in output power. The smaller the front facet reflectivity, the higher the threshold current. The optimal QW position needs to shift in the direction of a larger confinement factor to reduce the impact of the threshold current. It can be concluded that the maximum output power can be obtained by adjusting both the QW position and the front facet reflectivity.

Figure 7 shows the optimal QW position versus the injection current at R_{AR} = 0.01. It can be seen that the optimal QW position gradually shifts towards the p-side as the injection current increases. This is because the impact of threshold current on output power decreases as the injection current increases, and the effect of slope efficiency on output power increases relatively. The shift of the optimal QW position tends to be slow with increasing injection current. This is because the larger the value of p_x, the faster the threshold current increases, as shown in Fig. 4.

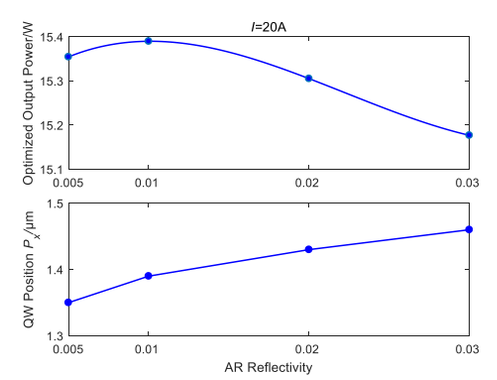

Fig. 6 The optimized output power and corresponding QW position versus the AR reflectivity
图6 优化后的输出功率和对应QW位置随AR反射率的变化

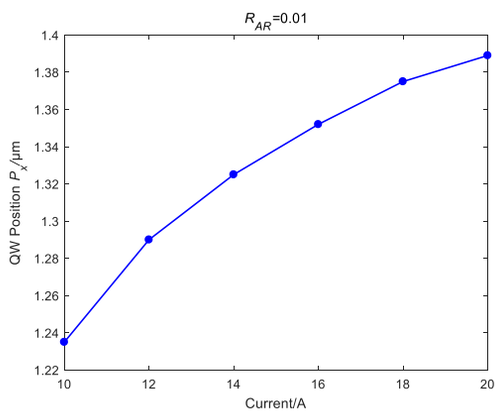

Fig. 7 The optimal QW position versus the injection current
图7 最佳QW位置随注入电流变化

Figure 8 illustrates the impact of losses on slope efficiency, threshold current and output power at I = 20 A and p_x = 1.39 μm. It can be seen that the threshold current and slope efficiency decrease with the increase of the front facet reflectivity in Fig. 8(a). Figure 8(b) shows that the output power increases monotonically with the decrease of the front facet reflectivity when LSHB is not considered. When considering LSHB, a decrease in output power occurs due to a higher threshold current and a more significant reduction in slope efficiency, as shown in Fig. 8(a). It is found that LSHB becomes the most significant factor in power reduction when the front facet reflectivity is low.

4 Summary

A simplified numerical analysis model is proposed to systematically analyze the impact of LSHB, TPA and FCA on the output characteristics of 1.06 μm long-cavity diode lasers. It is found that an appropriate reduction in the front facet reflectivity can increase the output power. But if the reflectivity is too low, it will cause severe LSHB, leading to a significant reduction in the slope efficiency and a notable increase in the threshold current, which in turn reduces the output power. For the same injection current, the QW position in the waveguide can be optimized to maximize the output power. The optimal QW position shifts towards the p-side as the front facet reflectivity or the injection current increases. LSHB becomes the most significant factor affecting the output power when the front facet reflectivity is low.

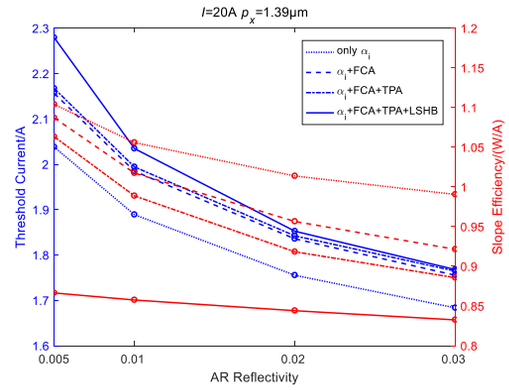

(a)

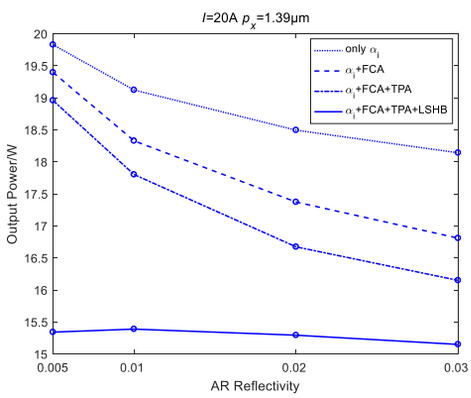

(b)

Fig. 8 Threshold current, slope efficiency and output power: (a) threshold current and slope efficiency versus the AR reflectivity; (b) output power versus the AR reflectivity

图8 阈值电流、斜率效率和输出功率:(a)阈值电流和斜率效率随AR反射率的变化;(b)输出功率随AR反射率的变化

References

[1] Chen Z, Bao L, Bai J, *et al*. Performance limitation and mitigation of longitudinal spatial hole burning in high-power diode lasers; proceedings of the Novel In-Plane Semiconductor Lasers XI[C]. SPIE, 2012: 245-252.

[2] Golovin V S, Shashkin I S, Slipchenko S O, *et al*. Longitudinal spatial hole burning in high-power semiconductor lasers: numerical analysis[J]. *Quantum Electronics*, 2020, **50**(2): 147-152.

[3] Rinner F, Rogg J, Friedmann P, *et al*. Longitudinal carrier density measurement of high power broad area laser diodes[J]. *Applied Physics Letters*, 2002, **80**(1): 19-21.

[4] Avrutin E A, Ryvkin B S. Effect of spatial hole burning on output characteristics of high power edge emitting semiconductor lasers: A universal analytical estimate and numerical analysis[J]. *Journal of Applied Physics*, 2019, **125**(2): 023108.

[5] Dogan M, Michael C P, Zheng Y, *et al*. Two photon absorption in high power broad area laser diodes; proceedings of the High-Power Diode Laser Technology and Applications XII[C]. SPIE, 2014: 131-137.

[6] Ryvkin B S, Avrutin E A. Asymmetric, nonbroadened large optical cavity waveguide structures for high-power long-wavelength semiconductor lasers[J]. *Journal of Applied Physics*, 2005, **97**(12): 123103.

[7] Ryvkin B S, Avrutin E A. Effect of carrier loss through waveguide layer recombination on the internal quantum efficiency in large-optical-cavity laser diodes[J]. *Journal of Applied Physics*, 2005, **97**(11): 113106.

[8] Juodawlkis P W, Plant J J, Donnelly J P, *et al*. Continuous-wave two-photon absorption in a Watt-class semiconductor optical amplifier[J]. *Optics Express*, 2008, **16**(16): 12387-12396.

[9] Abdullah D, Matthew P, Richard D, *et al*. 29.5 W continuous wave output from 100 μm wide laser diode; proceedings of the High-Power Diode Laser Technology and Applications XIII[C]. SPIE, 2015: 93480G.

[10] Kogelnik H. Theory of Dielectric Optical Waveguides[M]. Berlin: Academic Press, 1991: 15-79.

[11] Avrutin E A, Ryvkin B S. Theory of direct and indirect effect of two-photon absorption on nonlinear optical losses in high power semiconductor lasers[J]. *Semiconductor science and technology*, 2016, **32**(1): 015004.